Title

Analysis of synergies in converting underground storage sites: Natural gas to hydrogen with co-located CO2 storage

Journal

International Journal of Hydrogen Energy, 252

ISSN

0360-3199

Authors

Mouli-Castillo, Julien

Oldenburg, Curtis M

Zhang, Keni

et al.

Publication Date

2026-07-01

DOI

10.1016/j.ijhydene.2026.156158

International Journal of Hydrogen Energy 252 (2026) 156158

Contents lists available at ScienceDirect

International Journal of Hydrogen Energy

journal homepage: www.elsevier.com/locate/he

Analysis of synergies in converting underground storage sites: Natural gas to hydrogen with co-located CO_2 storage

Julien Mouli-Castillo [a,*], Curtis M. Oldenburg [c], Keni Zhang [c], Hanna Breunig [b]

[a] James Watt School of Engineering, University of Glasgow, Glasgow, G12 8QQ, UK
[b] Energy Analysis and Environmental Impacts Division, Lawrence Berkeley National Laboratory, Berkeley, CA, 94720, United States
[c] Energy Geosciences Division, Lawrence Berkeley National Laboratory, Berkeley, CA, 94720, United States

ABSTRACT

This study examines the untapped potential of synergistically converting underground natural gas storage (UGS) into underground hydrogen storage (UHS) with co-located CO_2 storage. Current approaches to subsurface storage technology (SST) development often prioritise single-use scenarios, overlooking the benefits of integrating multiple technologies. We investigate converting UGS assets into UHS through gradual cushion-gas injection over multiple years, rather than injecting all cushion gas in the first year, and include on-site CO_2 storage to offset site emissions. Mechanistic modelling shows this gradual transition reduces the Levelised Cost of Storage (LCOS) of H2 by 1.2-13.1% while retaining energy output within 3% of the current status quo. We also show that combined UHS and CO_2 storage hubs can reduce the LCOS of CO_2 by 45-77% for only a 3-10% increase in hydrogen LCOS relative to the status quo. This analysis framework may help future-proof SST sites and support a resilient, economically beneficial energy transition.

1. Introduction

Subsurface storage technologies (SSTs), which collectively encompass both subsurface energy storage and Geologic Carbon Sequestration (GCS, the storage component of Carbon Capture and Storage (CCS)), have emerged as central enablers for delivering the required reliability and security of supply for increasingly complex energy systems [1].

Foremost among these is subsurface energy storage, whose ability to shift terawatt-hours (TWh) of energy over hours to seasons offers the dispatchability that solar, wind, and tidal resources inherently lack. Alternative flexibility measures exist, but they all come with challenges. For example, demand response can entail costly curtailment payments, new grid-connections suffer from lengthy queues, and flexible nuclear power generation still awaits regulatory and economic resolution [2]; IAEA [3]. Long-duration energy storage (LDES) (i.e., over 10 h per day) therefore remains indispensable for power-system resilience during extreme weather events or unexpected outages [4]. Only porous rock reservoirs offer the physical scale and siting flexibility required for broad implementation of seasonal grid-scale storage [5,6]. Although no specific definition of “grid-scale” exists, the UK government and the U.S. Energy Information Agency both assume it relates to systems with an installed capacity greater than 1 MW [7,8]. In practice, subsurface energy storage technologies have power outputs of 100s to 1000s of GW, and offer discharge durations on the scale of hours to months [9,10].

A recent review of UHS options states that (pressure-) depleted natural gas reservoirs provide favourable storage conditions [11]. The same review notes that depleted gas reservoirs are generally cheaper to repurpose for UHS than oil reservoirs or saline aquifers. One approach to the conversion of an underground natural gas (mostly CH_4) storage (UGS) reservoir to underground hydrogen storage (UHS) is to start by injecting H_2, the bulk of which will become cushion gas during UHS operations. Following this priming of the system, stable operations assume a certain injection of H_2 and withdrawal of gases from the storage reservoir. Cushion gas is a necessary component of any kind of gas storage (e.g., natural gas, H_2, air) and serves to support reservoir pressure during withdrawal and ensure deliverability of stored gas. However, injection of a H_2 cushion gas is a very costly and time-consuming upfront investment.

Complementing energy storage, GCS delivers a permanent sink for the CO_2 waste stream captured from industrial processes and fossil-fuel power generation, and increasingly from direct-air capture [12,13]. Secure injection into storage complexes consisting of porous formations with overlying caprocks many hundreds of meters beneath the land surface provides long-term sequestration with minimal reversal risk [14,15]. Every recent global mitigation roadmap concludes that achieving the 1.5 °C or 2 °C temperature thresholds is implausible without large-scale CCS deployment [16].

Yet, while both subsurface energy storage and CCS are individually

* Corresponding author.
E-mail address: julien.mouli-castillo@glasgow.ac.uk (J. Mouli-Castillo).

https://doi.org/10.1016/j.ijhydene.2026.156158
Received 13 February 2026; Received in revised form 20 April 2026; Accepted 18 June 2026
Available online 25 June 2026

well studied, the potential synergies created when they are co-located and co-managed have been largely overlooked [17,18]. In one scenario of SST co-location, the storage of hydrogen and CO_2 would occur in distinct, vertically offset and isolated strata. In this scenario, the storage operations can be modelled financially as one project hub where costs and revenue streams such as carbon credits are evaluated together across the project lifespan.

To explore such SST synergies, we developed and modelled a novel case study in which a generic partially depleted natural gas field undergoes a phased conversion into a combined H_2 and CO_2 storage hub. Using these mechanistic simulation results, we then turn to the techno-economic performance of the conversion of a UGS facility to a UHS facility with and without co-located and co-managed GCS. The markers of synergy are estimated lower costs and/or quantifiably better overall performance. The first hypothesis we test in this work is: "Postponing the investment in cushion gas can yield comparable energy-storage performance while lowering the levelised cost of storage (LCOS)." In our analysis, we propose that gradually converting existing UGS facilities to UHS spreads the high upfront cost for H_2 cushion gas over a longer portion of the project's lifetime, thereby lowering the LCOS of the ultimate H_2 cushion. Deferring expenditure on cushion gas is feasible only if the reservoir continues to deliver at least the same quantity of recoverable energy throughout its operating life; any erosion of deliverability in an equivalent-energy sense could offset the short-term financial gain. To verify the evolution of energy deliverability during the conversion from UGS to UHS, we simulated the reservoir's mechanistic cycling behaviour in detail including tracking how pressure support, gas compressibility and phase interactions evolve over successive injection-withdrawal cycles to study how they alter the composition of the withdrawn gas. Such time-dependent simulations serve to reveal whether the phased emplacement of H_2 cushion gas compromises annual withdrawal rates, round-trip efficiency, or cumulative energy recovery.

The second hypothesis we examine is: "The addition of CO_2 storage at the site can lead to benefits from co-management." Operation of the facility is modelled as a defined annual cycle for energy storage operations and as a continuous injection of CO_2 for the CO_2 storage operations (the capture and transport to the site falls outside the system boundary for our analysis).

We use a set of LCOS metrics as a measure of techno-economic performance. Because LCOS is highly sensitive to assumed cycle count and capacity factor, we use it solely as an internal comparison metric between our studied scenarios. Direct comparison of LCOS results in this study against LCOS reported in other studies is unlikely to be possible unless one ensures all of the same key assumptions are made. As such, to ensure the global applicability of the study we investigated a range of electricity prices that captures the high and low end of diverse energy markets, such as the Nordics, the USA, and the European Union. Importantly this aligns with the geographical location of potential gas reservoirs for UHS [19] providing a level of consistency between the locations of relevant storage assets and the economic landscape.

Collectively, the literature indicates that deferring cushion-gas investment has the potential to lower LCOS but that a careful assessment of both the mechanistic energy storage performance and the offset of carbon emissions from natural gas is required. By focusing on partially depleted gas reservoirs and treating LCOS as an internal comparison tool, the proposed approach offers a pragmatic pathway to assess a cost-effective, low-carbon transition pathway from UGS to UHS.

2. Methodology

In this section we discuss the case study of transitioning a natural gas storage facility into a H_2 storage facility combined with CO_2 storage. We present both the reservoir model and the economic methods.

2.1. Surface facilities

Fig. 1A illustrates the principal components of the system. All components fall within the defined system boundary (red outline). The H_2 pipeline (1) delivers H_2 to and from the H_2 pipeline network. The CO_2 pipeline (2) supplies CO_2 to the system at a pressure sufficient for direct injection. The CO_2 injected by the system is captured off-site somewhere outside our system boundary. CO_2 is injected via the dedicated well (3) into a depleted gas reservoir (9). A separate H_2 intake pipe (5) delivers H_2 to a H_2 compressor (6), which compresses the gas to the required injection pressure due to the greater depth of the H_2 storage reservoir (10) (varies depending on the injection rate of each scenario presented in subsequent section). The gas mixture recovered from the H_2 store is purified via a pressure swing adsorption unit (7), ensuring separation and quality control of the H_2 stream. A H_2 return pipe (4) channels recovered H_2 back to the surface. Injection and recovery to and from the partially depleted gas reservoir (10) are managed by the H_2 well (8).

The co-location of SST, such as UHS and GCS, creates significant opportunities for operational and economic synergy through the shared use of key infrastructure and resources. In this context, synergy is defined by outcomes that demonstrate estimated lower costs and/or quantifiably improved overall performance compared to separately developed operations. In addition, a shared hub configuration can enable financial complementarity, whereby revenues generated from one process may be used to support the development, operation, or risk profile of another. These synergistic benefits are realised through the co-use and integration of several core elements, including:

- Land use and overall site footprint
- Personnel and operations staff
- Monitoring systems and reservoir surveillance
- Utility access
- Pipeline rights of way
- Well and pipeline engineering
- Emergency response equipment
- Planning, permitting, and reporting processes

Collectively, the integration of these components reduces duplication, streamlines workflows, and enhances coordination, while the potential for cross-support of revenue streams further strengthens the economic case. Together, these factors deliver measurable cost efficiencies and performance improvements that are indicative of synergistic co-located SST operations.

2.2. Conceptual storage complex model

We designed the storage complex model (Fig. 1) to simulate the co-location of SSTs that exploit an idealised dome-shaped geological structure with multiple reservoir-seal layers. We configured the system with alternating reservoir and sealing formations to ensure structural integrity and containment of the injected gases. We separated a shallow natural gas reservoir (Fig. 1B, R1), 50 *m* thick, from a deeper natural gas reservoir (Fig. 1B, R2) of the same thickness with a 200 m-thick caprock (Fig. 1B–S2), which provides a natural barrier to vertical fluid migration. Assuming a formation with a history of gas containment and safe reservoir engineering, we did not further evaluate possible effects of faults or well or pipeline failures.

We modelled the storage system using two separate simulations: one focused on the shallow reservoir used for carbon storage, and the other on the deeper reservoir used for H_2 storage. The two-simulation approach is justified by the large thickness (200 *m*) of the continuous seal (Fig. 1B–S2) between the two reservoirs (Fig. 1B, R1 and R2) which prevents heat and mass flow over operational time scales. We included open boundary conditions in the radial direction to model the flow of mass and energy to and from the connected aquifer system connected to the gas legs of the reservoirs. We set the system initially at hydrostatic

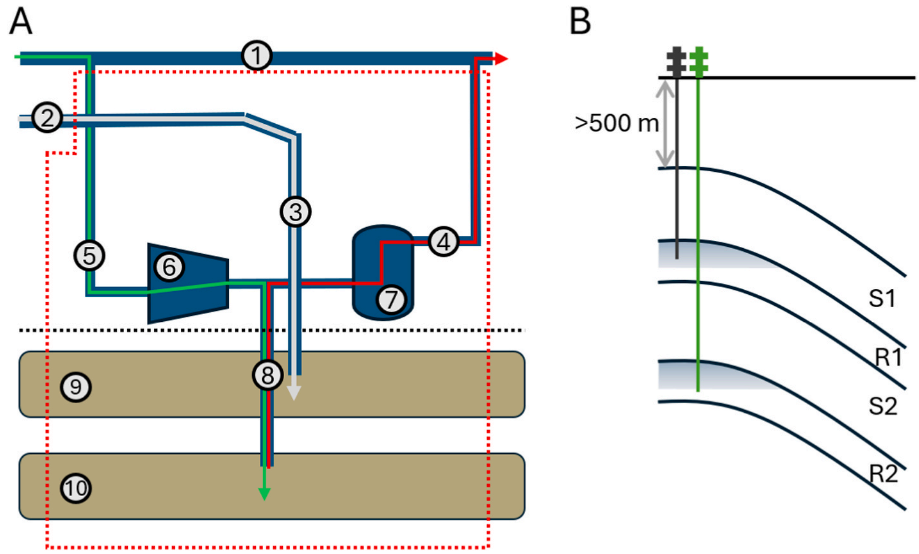

Fig. 1. A) Diagram of the system components. 1, H_2 pipeline; 2, CO_2 pipeline; 3, CO_2 injection well; 4, H_2 return pipe; 5, H_2 intake pipe; 6, H_2 compressor; 7, gas purification via pressure swing adsorption; 8, H_2 well; 9, shallow reservoir; 10, deep reservoir; red outline represents the system analysis boundary; B) Conceptual model of the storage complex. S1 is the shallow seal, R1 the shallow depleted gas reservoir where CO_2 is stored, S2 the deeper seal, R2 the deeper partially depleted gas reservoir where H_2 is stored. The grey well is the CO_2 injection well and the green well the hydrogen injection and withdrawal well. (For interpretation of the references to colour in this figure legend, the reader is referred to the Web version of this article.)

pressure, with each reservoir containing a 30 *m* thick gas zone at its top with ~40% CH_4 gas saturation (Fig. 2). The average structural dip of the geological formations in the horizontal distance covered by the gas cap is 3°. We set the crestal depth of the shallow reservoir at 720 *m*, and that of the deeper reservoir at 970 *m*. This choice served to allow supercritical CO_2 ($scCO_2$) storage while avoiding deep drilling and related costly well completions. We set the mass fraction of CH_4 in the reservoir to 0.98 CH_4 and 0.02 H_2 to improve numerical stability, while the rest of the model was fully saturated with water. We included two wells to control the injection and withdrawal of gases: the CO_2 well is screened over the top 30 *m* of the shallow reservoir (Fig. 1B, R1), and the H_2 well is screened in the top 30 *m* of the deep reservoir (Fig. 1B, R2). These wells have a diameter of 0.66 *m* which is consistent with values used in prior subsurface gas storage modelling studies and represents a realistic large-diameter completion while remaining computationally tractable [20]. This conceptual framework provides a representation of a multi-layered subsurface storage system, supporting our investigation of synergistic H_2 and CO_2 storage strategies. (Interested readers can find files containing initial conditions and model input properties and parameters in ESI.)

The assumptions outlined in Table 1 ensure that all scenarios are evaluated within a consistent, integrity-preserving operating envelope. By constraining operations to remain below fracture pressures, excluding caprock failure and well-integrity loss, and assuming standard

Table 1
Constraints and assumptions related to the subsurface system.

Constraint category	Assumption
Pressure limits	Operation remains below fracture pressure (H_2: ~97–109 bar vs ~183 bar limit; CO2: ~73–83 bar vs ~136 bar limit).
Caprock integrity	Continuous sealing formations; ~200 *m* caprock prevents vertical migration; no fault activation considered.
Well integrity	Dedicated wells (0.66 *m* diameter, 30 *m* screens) assumed fully intact; no leakage, cross-flow, or failure.
Monitoring	Standard monitoring assumed (pressure, composition, well integrity). In part due to assumed UGS operations prior to the start of the time window considered.

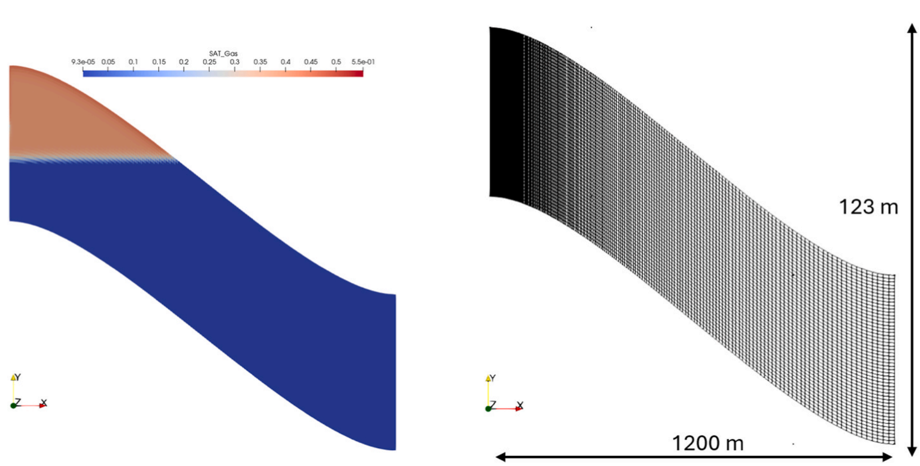

Fig. 2. Left: Initial gas saturation in the UHS reservoir showing the gas cap. Note the horizontal scale has been reduced by a factor of 10. Right: Spatial discretisation using GMSH.

monitoring across all cases, the analysis isolates the effect of cushion-gas scheduling on system performance and cost. As a result, the reported LCOS differences reflect variations in injection timing, energy recovery, electricity market, and discounted cash flow rather than differences in geomechanical risk, containment performance, or operational reliability. While these simplifying assumptions may influence absolute cost estimates in a site-specific deployment, they are applied uniformly across all scenarios and therefore do not alter the relative comparison between cushion-gas emplacement strategies.

2.3. Processes & numerical implementation

The storage and injection dynamics are governed by mass and energy conservation equations that model the two-phase flow and mass transfer of the gas and liquid phases and their various chemical components, respectively, along with heat transfer between the fluid phases and the reservoir rocks. The model simulates two-phase Darcy flow of gaseous and aqueous fluids in porous media with the mass components water (H_2O), H_2, CH_4, and CO_2 distributed in the two phases based on their solubilities. The flow model includes capillary and buoyancy effects which influence gas migration and retention as controlled by residual gas saturation. The simulation also accounts for mass diffusion processes which play a role in gas mixing (with implications for purity of withdrawn H_2).

The mass and energy conservation equations are solved using the Integral Finite Difference Method (IFDM) with implicit time-stepping as implemented in TOUGH4, a modernised and thoroughly updated version of the widely used TOUGH codes [21]. The TOUGH codes have been widely used for predictions of CO_2 injection, migration, and storage feasibility [22,23], for natural gas storage including its coupling to geomechanical models [24] and to wellbore flow [25,26], and more recently for H_2 storage [27].

TOUGH4 is used here to simulate multiphase flow and transport of water, brine, and the multicomponent gas mixtures where transport occurs by advection and Fickian diffusion. The EOS7 (equation of state module) in TOUGH4 extends and consolidates the older EOS7, EOS7R, EOS7C, and EOS7CA modules. EOS7 calculates real gas mixture properties (density, enthalpy, viscosity) using a choice of cubic equations of state (Peng–Robinson, Redlich–Kwong, or Soave–Redlich–Kwong) along with specialised methods for viscosity of H_2 mixtures. TOUGH4 and EOS7 model single- and two-phase conditions with up to 11 components (water, brine, up to four gases, tracers), and optional processes including molecular diffusion, salinity effects, biodegradation, wellbore flow, and non-isothermal simulations. Interested readers are encouraged to peruse the user guide (EOS7 | TOUGH4 User Manual).

For the generic analyses of synergies which are the focus of this study, we assume the domain is axisymmetric around the injection/withdrawal well. The top and lower boundaries are closed to mimic sealing formations. We set the outer (right-hand side) boundary to be open by setting constant properties. We model the wellbores as high-permeability cells with a permeability of 1×10^{-9} m^2. We discretised the domain into a grid of 250 cells in the lateral direction and 50 cells in the vertical direction using PyGMSH [28]. We specified a geometrically increasing radial cell size outward from the well and uniform thickness of the cells. This gentle widening in the radial direction provides detailed resolution around the well screen while keeping the overall number of cells computationally manageable on a desktop. We set the initial temperature using a geothermal gradient of 33 °C km^{-1} and a temperature of 8.9 °C at 0 *m* depth.

2.3.1. Rock and fluid properties

We model the fluid properties in this system using the Soave-Redlich-Kwong (SRK) equation of state (EOS) option in EOS7, which provides an accurate prediction of fluid properties and phase behaviour under reservoir conditions, particularly for H_2 [29]. We assign permeability, thermal conductivity, heat capacity, and density based on values reported for sandstone used in previous energy storage modelling work [20]. We assign reservoir cells a porosity of 0.10 to provide a conservative pore volume for seasonal storage, while the well cells are assigned an artificially high porosity (0.95) and permeability (10^{-9} m^2) to allow fluid injection with minimal resistance while maintaining solver stability.

Relative permeability is modelled as shown in Table 2 by the Corey curves (TOUGH4 IRP = 3) and a van Genuchten law (TOUGH4 ICP = 7) for capillary pressure [30,31]. We set residual liquid saturation, Slr, to 0.37 to leave an immobile water amount in the gas cap. A residual gas saturation, Sgr, of 0.29 is set in the matrix to mimic the gas fraction that is unable to leave the smallest pores or inaccessible pores of the rock [32]. Sgr is set to 0.01 in the wells for stability. These relative permeability and capillary pressure parameters were chosen based on a pore-size index, λ, of 0.5 which suits a well-sorted sandstone, and the assigned entry-pressure and maximum-pressure values ($P_0 \approx 12$ kPa, *Pc* max = 100 kPa) are within the range measured for sandstones [32,33].

2.4. Simulation scenarios

We carry out mechanistic simulations to evaluate whether staggering the emplacement of the cushion gas in a partially depleted gas field can lead to a reduction in LCOS sufficient to cover the cost of co-located CO_2 storage. To test the effects on storage performance and cost of staggering cushion gas emplacement, we developed four mechanistic scenarios of the UHS and one for the CO_2 storage. Only one mechanistic simulation (E) is required for the CO_2 storage as it is functionally independent of the UHS operations. The four UHS scenarios include (A) a reference case, where all the cushion gas is injected within the first year; scenarios (B), (C), and (D) emplace cushion gas over 2, 5, and 10 years, respectively (Table 3). We achieve the spreading of the cushion gas by injecting an equal fraction of the cushion gas during every annual injection phase of

Table 2
Domain properties. Permeability, thermal conductivity, heat capacity and density are representative of a sandstone reservoir [20]. Porosity is chosen to represent a reservoir with moderate pore volume available for storage. The well cells (injection/withdrawal cells) are set to a very high porosity and permeability to model relatively unimpeded flow relative to the reservoir rock whilst avoiding numerical instability. See the TOUGH4 documentation for additional descriptions of the Relative permeability and capillary curve parameters: ICP = 7 van Genuchten function | TOUGH4 User Manual, IRP=3 Corey's curves | TOUGH4 User Manual.

Parameter	Reservoirs	Boundary	Wells
Subdomain Parameters			
Density ($kg\ m^{-3}$)	2600	2600	2600
Porosity (–)	0.10	0.10	0.95
Permeability X (m^2)	1.0×10^{-12}	1.0×10^{-12}	1.0×10^{-9}
Permeability Y (m^2)	1.0×10^{-12}	1.0×10^{-12}	1.0×10^{-9}
Permeability Z (m^2)	1.0×10^{-13}	1.0×10^{-13}	1.0×10^{-9}
Thermal Conductivity ($W\ m^{-1}\ K^{-1}$)	2.51	2.51	2.51
Heat Capacity ($J\ kg^{-1}\ K^{-1}$)	920	920	920
Relative Permeability Curves Parameters			
RP (1) — Slr (–)	0.37	0.37	0.37
RP (2) — Sgr (–)	0.29	0.29	0.01
Capillary Pressure Curve Parameters			
CP(1) — λ (–)	0.50	0.50	0.50
CP(2) — Slr (–)	0.35	0.35	0.35
CP(3) — $1/P_0$ (Pa^{-1})	8.0×10^{-5}	8.0×10^{-5}	8.0×10^{-5}
CP(4) — P_{max} (Pa)	1.0×10^5	1.0×10^5	1.0×10^5
CP(5) — Sls (–)	1.0	1.0	1.0
Geometry Parameters			
Thickness of Reservoirs (m)	50	-	-
Shallow Well Screen Length (m)	-	-	30
Deep Well Screen Length (m)	-	-	30
Average Dip Angle (°)	3	-	-

Table 3
Description of the model runs performed in this study.

Scenario	Cushion gas injection period (year)	Normal injection rate (kg s^{-1})	Excess injection rate (kg s^{-1})	Total injection rate (kg s^{-1})	Gas	Compressor Power (MW)
(A)	1	1.00	2.00	3.00	H_2	0.50
(B)	2	1.00	1.00	2.00	H_2	0.45
(C)	5	1.00	0.40	1.40	H_2	0.41
(D)	10	1.00	0.20	1.20	H_2	0.40
(E)	N/A	3.17	N/A	3.17	CO_2	0.10

the cycle. This excess injection is defined as the excess rate of mass injection that is used above that which would be needed to exactly balance the withdrawals. Following the injection of the cushion gas, the injection rate defaults back to 1 kg s^{-1} for all scenarios, which results in equal net annual withdrawal and injection. The withdrawal rate is set to 11.1 $stdm^3\ s^{-1}$ in all scenarios to ensure a constant volume is withdrawn even with variations in the gas composition. Note that the withdrawal rate has to be specified in volumetric terms since a mixture with variable composition is withdrawn from the reservoir. The selected injection and withdrawal rates are aligned with reported deliverability from existing gas storage facilities of comparable scale (e.g. Humbly Grove, UK), ensuring that the simulated operating pressures remain within acceptable limits and representative of seasonal storage operation. We set the injection of CO_2 in the shallow reservoir (a single scenario E) at a rate of 0.1 MT y^{-1} (3.17 kg s^{-1}) during the entire year. This rate is chosen to avoid a spillover of CO_2 from the structure.

2.5. Economic model

2.5.1. LCOS calculation

The economic analysis considers the following economic scenarios presented in Table 4: (1) & (3) A baseline series, where only UHS costs are considered for each of the A, B, C and D mechanistic scenarios and the CO_2 storage operations (E) are assumed not to take place. (2) & (4) A comparative series, where both UHS and CO_2 operations (E) are considered for each A, B, C and D mechanistic scenario. (1) & (2) Assume a market with high electricity costs (e.g., E.U. and UK) and (3) & (4) a market with low electricity costs (e.g., Nordics, India, USA) [34]. The high-electricity-cost case samples a normal distribution with a mean of 95 €/MWh (σ = 5 €/MWh) and the low-electricity-cost case with a mean of 35 €/MWh (σ = 5 €/MWh).

We evaluate the economic viability of UHS for subsurface energy storage with and without CO_2 storage through the LCOS of energy, mass of H_2 and mass of CO_2 (when CO_2 storage is considered in economic scenario series (2) and (4)), using the Net Present Value (NPV) method over a project lifetime of 40 years, accounting for capital and fixed and variable operating (OPEX) expenditures. We define LCOS as follows:

$$LCOS_{\varphi} = \frac{PV_{CAPEX} + PV_{OPEX}}{PV_{\varphi}} \quad \text{Eq. 1}$$

Where the PV expanded terms are:

$$LCOS_{\varphi} = \frac{\sum_{t=0}^{N} [CAPEX_t + OPEX_t] \frac{(1+i_f)^t}{(1+i)^t}}{\sum_{t=0}^{N} \varphi_t \frac{1}{(1+i)^t}} \quad \text{Eq. 2}$$

Where, t is the time period (year), N the maximum number of periods considered, i_f the inflation factor, i the discount rate, φ the quantity in which to express the LCOS. φ is varied to be MWh of recovered energy from withdrawn gas using CH_4 and H_2's Higher Heating Value (consistent with UK national energy statistics and providing LCOS in €/MWh), tonnes of recovered H_2 (providing LCOS in €/kg_{H2}), or net tonnes of stored CO_2 (providing LCOS in €/$kgCO_2$). We note that the net stored CO_2 is computed only to capture the variations in emissions resulting from the on-site storage operations (i.e., the withdrawal of CH_4). In other words, external factors like carbon intensity of the electricity or embedded carbon from construction and manufacturing of equipment are not considered.

Our approach for deriving CAPEX and OPEX terms are detailed in Supplementary Information and summarised briefly in the following sections. All cost inputs were first harmonised to a common EUR 2024 basis before entering the LCOS model. The annual CAPEX and OPEX cash flows were then escalated using a fixed annual inflation factor of 2.5% (i_f) and discounted using the scenario discount rate (i), such that the reported LCOS values are based on nominal cash-flow NPVs referenced to a common 2024 price basis. Any conversions of USD to EUR are done using an exchange rate of 0.85, which is representative of the exchange rate in Q4 2024. Prior to the conversion to euros all USD costs have been adjusted to USD 2024 values using the CPI Inflation Calculator (www.officialdata.org/us/inflation/2012).

2.5.2. TEA model system boundaries

For the LCOS calculations, the system boundary includes the on-site UHS infrastructure and operations: cushion-gas supply, the H_2 storage well, on-site piping, H_2 compression, PSA gas purification, and operating labour. In the multi-use cases, the boundary additionally includes the CO_2 storage well and CO_2-storage operating costs. H_2 production and electricity supply are treated exogenously through input prices rather than as process units within the model, while CO_2 capture, transport to site, and CO_2 compression are excluded from the reported LCOS totals; accordingly, the CO_2 stream is treated as arriving at the facility at injection-ready pressure. Specific boundary conditions are specified in the sections below. The end-use of the recovered methane is not considered here as it is a site-specific issue, however the emissions associated with that methane are accounted for by assuming every

Table 4
Description of economic analysis scenario series.

Economic Scenario Series	Description	Technologies considered	Factored into the LCOS cashflow	Electricity Cost Scenario	Mechanistic Scenarios Used
(1)	Baseline, UHS without CO_2 storage	UHS	Costs of UHS	High Cost	A, B, C, D
(2)	UHS and CO_2 storage LCOS	UHS, CO_2 storage	Costs of UHS and CO_2 storage	High Cost	A, B, C, D, E
(3)	Baseline, UHS without CO_2 storage	UHS	Costs of UHS	Low Cost	A, B, C, D
(4)	UHS and CO_2 storage LCOS	UHS, CO_2 storage	Costs of UHS and CO_2 storage	Low Cost	A, B, C, D, E

kilogram of methane will produce 2.7 kg of CO_2.

2.5.3. Cushion gas delivery and cost

We calculate the cost of cushion gas by summing the respective costs of H_2 multiplied by its required mass:

$$CAPEX_{\mathrm{cushion}} = cost_{H_2} \times m_{H_2,cushion} \quad \text{Eq. 3}$$

where costs are given in EUR per unit mass, and the final cost is converted to million euros (MEUR). The cushion gas injected is pure H_2, hence this is what is considered a project cost in Eq. (3). Once it is injected into the reservoir it will mix with the CH_4 already in place. Our mechanistic simulations account for the effects of that mixing on the system's performance.

The cost of H_2 is correlated to the electricity price of the scenario because cushion gas is assumed to be supplied by PEM electrolysis, for which electricity is a major but not the only cost contributor:

$$cost_{H_2} = \frac{\mathrm{cost}_{electricity}}{g(\mathrm{cost}_{electricity}, i)} \frac{39.44}{1000} \quad \text{Eq. 4}$$

Where g is a function expressing the ratio the cost of electricity to the price of H_2 for a proton exchange membrane (PEM) electrolyser. It assumes a capacity factor of 50% and uses a correlation between the electricity cost and discount factor, i, based on a dataset provided by National Electricity System Operator of the UK [35]. The electricity provided to the system falls outside the model boundaries, so we use an average value between grid and renewables for the capacity factors. The second term is a factor to convert from €/MWh to €/kg_{H2}. This formulation allows H_2 cost to vary with both electricity price and discount rate rather than assuming a fixed linear pass-through. Sensitivity to this assumption is therefore represented in the Monte Carlo analysis through variation in electricity price and discount rate, whereas the electrolysis energy requirement, PEM configuration, and capacity factor remain fixed in this study.

2.5.4. Piping costs

We model the CAPEX for H_2 and CO_2 transport around the site using a framework designed for H_2 production facilities (Fig. 1 A. Figs. 2, 4, and 5) [36], considering the pipeline length (L) and (mass) flow capacity (Q):

$$CAPEX_{pipe} = 600 \cdot (Q/Q_0)^{0.48} \cdot (L/L_0)^{0.24} \cdot L \quad \text{Eq. 5}$$

where (Q_0) and (L_0) are reference conditions (16,000 tonnes/day and 100 km respectively).

We model annual OPEX for piping as 4% of the CAPEX [36]:

$$OPEX_{pipe} = 0.04 \cdot CAPEX_{pipe} \quad \text{Eq. 6}$$

The limitations here include assumptions of standard installation conditions, as we assume a region with natural gas storage has established pipeline right-of-way pathways that avoid challenging terrains or prohibitively expensive regulatory conditions.

2.5.5. Subsurface costs

Drilling and operational costs for wells (Fig. 1 A. Figs. 3 and 8) are determined using an exponential depth-dependent cost function to capture the non-linearity of drilling cost with respect to depth [37]. The model is parameterised by percentiles, reflecting uncertainty in well-drilling costs. For the purposes of this study, we use the P50:

$$C_{new\ well} = a \cdot e^{b \cdot d} \quad \text{Eq. 7}$$

where $C_{new\ well}$ is the cost of a new well, (a) and (b) are percentile-specific parameters provided in Table 5 ((a) is in MEUR and (b) is in m^{-1}), and (d) is the well length, proxied as the reservoir depth at which the well enters the reservoir formation (meters). Costs for reused wells are assumed to be one-quarter of new wells [38], reflecting typical savings in re-entry operations. We assume the wells consist of reused wells undergoing a workover. Total CAPEX for a number of reused wells (n_{reused}) is given as:

Table 5
Constants used to produce the well cost curves for different percentiles using Eq. (7) [37]. *Asterisk indicates values used in our study.*

Percentile	a (MEUR)	b (m^{-1})
Pmin	3.09	2.06E-4
P10	3.54	2.39E-4
P50*	3.56	2.72E-4
P90	4.78	3.25E-4
Pmax	4.78	3.13E-4

$$CAPEX_{wells} = n_{reused} \cdot \frac{C_{new\ well}}{4} \quad \text{Eq. 8}$$

We model annual OPEX as a base cost of 0.5 MEUR per well, based on previous literature.
[39]:

$$OPEX_{wells} = n_{wells} \cdot OPEX_{per\ well} \quad \text{Eq. 9}$$

The CO_2 storage infrastructure (Fig. 1 A. Figs. 2 and 3) incorporates the geological reservoir, and well system. We assume that the CO_2 is delivered to the facility at 80 bar via pipeline, hence it is at sufficiently high pressure to be injected into the geological reservoir without compression, and the well and associated O&M are designed to achieve the specified storage target.

CO_2 storage CAPEX is derived based on the CO_2 injection well costs as described previously where operational costs incorporating fixed maintenance (O&M) and storage fees per mass unit of CO_2 [40] are computed as:

$$OPEX_{CCS} = m_{\mathrm{CO2}} \cdot C_{\mathrm{O\&M,storage}} \quad \text{Eq. 10}$$

2.5.6. Compressor system costs

Compressor (Fig. 1 A. Fig. 6) CAPEX estimation employs the following model [41] which has been demonstrated to be suitable for geological H_2 storage system economic models [39]:

$$CAPEX_{compressor} = f \cdot \left(P_{compressor} \times 10^3\right)^{0.82} \quad \text{Eq. 11}$$

where f is an empirical factor set to 2491, and $P_{\mathrm{compressor}}$ is the compressor power rating in MW obtained from using the peak H_2 injection pressure of the mechanistic simulation (Eq. (12)). Specifically, the compressor pressure is given by

$$P_{compressor} = sm \frac{kR}{k-1} T_1 \left[\left(\frac{p_2}{p_1} \right)^{\frac{k-1}{sk\eta_p}} - 1 \right] \quad \text{Eq. 12}$$

where p_1 is the inlet pressure, taken as the delivery pressure of the pipeline set to 80 bar (8×10^6 Pa), p_2 is the outlet pressure set to the maximum injection pressure encountered at the wellhead obtained from the mechanistic models (Pa), and s is the number of identical compression stages (dimensionless). k is the ratio of specific heats (dimensionless), and R is the specific gas constant J $kg^{-1}K^{-1}$. The parameter η_p is the polytropic efficiency (dimensionless). The temperature T_1 (K) is the inlet temperature at each stage, assumed to be restored by intercooling or reheating. The $P_{\mathrm{compressor}}$ obtained for each scenario are summarised in Table 3.

We determine OPEX based on the cost of electricity and a fixed maintenance fee of 3% [42]:

$$OPEX_{compressor} = A_0 \cdot H_{year} \cdot \frac{C_{el}}{\eta_{comp}} \cdot P_{compressor} + b \cdot CAPEX_{compressor} \quad \text{Eq. 13}$$

where the availability of the compressor is given by A_0, the number of hours in a year is H_{year}, C_{el} is the cost of electricity, η_{comp} is the compressor efficiency, and *b* represents operational and maintenance parameters.

2.5.7. Gas purification by pressure swing adsorption (PSA) system costs

In our study we do not include the cost of conversion back to electricity as we do not want to pre-suppose an end-use. It is likely that H_2 stored at this scale will be used to support the energy grid management on a national or regional scale and will therefore be directed towards energy networks rather than directly towards a specific end-user, although H_2 hubs proposed in the US suggest coupling with industrial end users. This is why we compute the energy from withdrawn mass using the Higher Calorific Value of H_2 and CH_4. The reason why we incorporate the gas purification step in our study is two-fold. First, it is likely that gas purification will be required in one way or another before the withdrawn gas is used. Hence, removing this step entirely would artificially reduce the LCOS. Second, there is a case to be made that there is more value in obtaining two purified gas streams, one of H_2 and the other of CH_4. Numerous methods for gas purification allow for the pressurisation of at least one of the streams, which is useful for pipeline transport [43,44]. This remains compatible with the idea that the energy in both streams remains valuable and could be used or sold. Finally, we use a generic approach to estimate the costs of purification as the future regulations and standards around gas composition in energy networks are constantly evolving, hence, a detailed process model is not warranted in the context of our analysis.

We model gas clean-up as a pressure swing adsorption (PSA), due to its technical maturity and ability to achieve fuel cell level purities (Fig. 1 A. Fig. 7), with unit costs determined from a reference flow rate and adjusted by a scaling exponent (0.66) [45] according to:

$$CAPEX_{PSA} = C_{ref} \cdot \left(\frac{Q_{PSA}}{Q_{ref}} \right)^{0.66} \quad \text{Eq. 14}$$

with (C_{ref}) as reference cost and (Q_{PSA}), (Q_{ref}) the PSA flow rates. OPEX incorporates periodic adsorbent replacement costs (activated carbon and zeolite) [39]:

$$OPEX_{PSA} = \frac{cost_{AC} \cdot m_{AC} + cost_{ZE} \cdot m_{ZE}}{replacement\ rate \cdot 10^6} \quad \text{Eq. 15}$$

Although the model presumes stable operating conditions and predictable adsorbent lifetimes, potentially disregarding cost fluctuations due to variable impurity levels or operational disruptions.

2.5.8. Ancillary costs (administrative, construction, overhead, labour)

The ancillary costs are handled in two different ways dependingon whether they are related to the construction and installation of the components, which fall within the Overnight Capital Cost (OCC) of the first year, or whether they are recurring costs that happen throughout the project lifetime and warrant being included as an operational expenditure.

The proportion of these costs associated with OCC are evaluated using an established method [46] of estimating the cost of purchased-equipment installation, instrumentation & controls (installed), piping (installed), electrical (installed), buildings (including services), yard improvements, service facilities (installed), land, engineering & supervision, construction expense, contractor's fee, and contingency. In the approach, the estimates are based on the purchased equipment cost, which is obtained using the CAPEX equations above for the specific pieces of equipment detailed in Fig. 1. Timmerhaus, 1991, provides in their Table 4, a range for each of those costs. Once a value in those ranges is selected using random sampling, the values are normalised and used to compute the cost associated with each category.

2.5.9. Uncertainty and sensitivity analysis

We use Monte Carlo simulations to capture the impacts on LCOS of parameter uncertainty. The Monte Carlo Analysis is performed by sampling the parameter distributions shown in Table 6 ,000 times through a custom Python model that implements the economic model presented above. At this sample size, the resulting output distribution is fully converged, with the P10, P50, and P90 values remaining identical to two significant figures across repeated runs.

2.5.10. Limitations and validity considerations

The combined numerical simulation and economic modelling uses a conceptual model that reduces computational burden. Specifically, a TOUGH4 mechanistic model large enough to capture the key physical processes of gas storage while also small enough to execute efficiently was used to simulate cyclic injection and withdrawal in the stacked storage system. We derive the LCOS denominators (mass of H_2 recovered, energy recovered and net CO_2 stored) from the five mechanistic scenarios (A), (B), (C), (D), and (E). The single-well is small relative to a large field project making unit costs conservative; larger multi-well fields would gain economies of scale. Even so, the well-reservoir system samples retain a fixed set of physical properties with different injection schedules based on the scenarios and the economic model explores the full uncertainty space for the cost of H_2 and electricity, discount rate, and annual storage OPEX.

Cost estimates rely on literature correlations and simplified assumptions about reuse, flow rates, and equipment life. Real sites may differ owing to geology, permitting, supply chains and policy, so project-specific studies remain essential. Despite these caveats, the linked UHS–CCS model works as a proof-of-concept to explore cost drivers, trade-offs and the strategic value of co-located H_2 and carbon storage.

3. Results

3.1. Annual energy production

Scenario A (base case). Fig. 3 indicates that energy content of the first withdrawal of gas after the whole CG is injected in year 1 yields roughly a petajoule (represented as a negative value due to removal from storage). The system then rapidly enters a stable operating regime in which the energy content of annual withdrawals remains effectively constant over the remainder of the simulation, yet marginally greater than in the first year. As can be seen, mixing gradually occurs and CH_4 contributes more to the energy mix before reducing again as any residual mobile CH_4 has been removed from the reservoir. Variability around the mean is small, and only a negligible decrease in energy output is observed,

Table 6
Parameter Distributions used in the Monte Carlo analysis. Annual Well OPEX is the estimated fixed annual OPEX per well in MEUR. n is the number of years of the project. Cost of Electricity is the cost of electricity for the compressors. Truncnormal refers to a truncated normal distribution that keeps resampling the distribution until all samples fall within the superimposed min-max range, which is useful to avoid non-physical samples and unrealistic accumulation of min and max values. All constant parameters and conversion factors applied are provided as supplementary information.

Parameter		Distribution	Details	Rationale
Cost of Electricity (€/MWh)	High cost	Truncnormal	Mean: 95.0; Std. Dev.: 5.0; Min.: 80.0; Max.: 110	[34]
	Low cost	Truncnormal	Mean: 35.0; Std. Dev.: 5.0; Min.: 20.0; Max.: 50	[34]
Discount Rate		Truncnormal	Mean: 0.085; Std. Dev.: 0.013; Min.: 0.06; Max.: 0.115	Comparable with rates found for energy infrastructure projects ([47]; [48]; [49];[50])
CO_2 storage O&M cost (€/kg_{CO2})		Truncnormal	Min.: 5.27E-3*0.9; Max.:5.27E-3*1.1	+/−% variation from Ref. [40] value

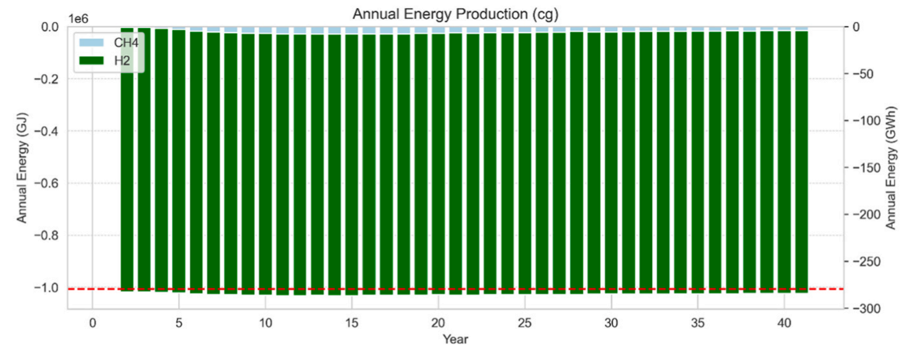

Fig. 3. Annual energy outputs from Scenario A – given as negative values if removed from the store. The current status quo approach is the case where all the cushion gas is injected in the first year. The dashed red line indicates the amount of energy that would be withdrawn if all the withdrawn gas was pure H_2. Because CH_4 has a higher volumetric energy density than H_2, the energy output of the withdrawn gas mixture is always higher than if the gas were pure H_2. (For interpretation of the references to colour in this figure legend, the reader is referred to the Web version of this article.)

consistent with a near–steady-state response once the storage system had been conditioned. Across this stable phase, CH_4 represented only a 2.46 ± 0.69% of the delivered energy stream, contributing a small and persistent share relative to the dominant H_2 carrier. Notably, the energy output of withdrawn gas is always higher (larger negative number) than if the same volume of pure H_2 was withdrawn (red line).

Scenario B (2 year case). Fig. 4 shows that, during the 2 years of CG injection, withdrawals are similar in magnitude to those of the base case but less energy is recovered in the second cycle than the first. During this initial charging interval, CH_4 contributes 0.6 ± 0.7% of the overall energy output. Once the system is fully primed from year 3 onwards, withdrawals converge tightly on the same stable rate observed in the base case. In this subsequent steady phase, the methane contribution increases to a level consistent with the base case and remains comparably stable.

Scenario C (the 5 year case). Fig. 5 shows that, during the period of cushion gas injection, more net energy is withdrawn at the start of the period. The net energy withdrawn decreases over the 5 year period. This pattern is consistent with declining mobilisation of residual CH_4 as the system approaches a primed state with all the CG injected. After the transition to a balanced operation between injection and withdrawal, the withdrawn energy converges closely on the same long-run value seen across the previous scenarios. CH_4 then stabilises at 2.64 ± 0.59%, a modestly higher share of the produced energy than in the base case.

Scenario D (the 10 year case). Fig. 6 shows that the effect observed in Scenario C is more pronounced with the first cycle leading to the most energy withdrawn (about 3% more than in the first cycle of the base case) followed by a decline in energy withdrawn as more H_2 CG is injected into the system. CH_4 accounts for the largest and most variable share of the energy stream (3.67 ± 2.52%) during this first decade of CG injection. Once all the excess injection has taken place and the CG is in place, withdrawals rapidly approach a plateau that closely matches the stable rates observed in the other scenarios. CH_4 contribution to withdrawn energy contracts from its elevated initial values and settles into a relatively steady level at 2.33 ± 0.48% that is slightly lower than the base-case steady-state contribution due to less CH_4 remaining in the store due to its greater withdrawal during the decade of CG injection.

3.2. LCOS Monte Carlo analysis results

Figs. 7 and 8 present the LCOS for H_2 in terms of H_2 mass (€/kgH_2) or energy (€/MWh). In Fig. 8, the LCOS is also presented in terms of net CO_2 stored (€/kgCO_2). Fig. 7 reports the values for the UHS single-use economic scenarios (1) and (3) and Fig. 8 for the multi-use economic scenarios (2) and (4). Each scenario is evaluated for the CG injection durations of 1, 2, 5, and 10 years from our mechanistic scenarios A, B, C, and D. Error bars represent P10–P90 ranges, and annotations indicate median (P50) values above each point and relative reductions compared to the 1-year case below each point.

3.2.1. UHS Single Use

For LCOS (€/kgH_2), the high-electricity-cost scenario (1) exhibits values decreasing from 2.54 €/kgH_2 when all the CG is injected in Year 1 to 2.25 €/kgH_2 when its injection is spread over ten years, while the low-electricity-cost scenario (3) ranges from 2.01 €/kgH_2 to 1.83 €/kgH_2 over the same period. The corresponding energy LCOS (€/MWh) follows a similar trend, with the high-electricity-cost scenario (1) decreasing from 63.22 to 54.95 €/MWh and the low-electricity-cost scenario (3) from 49.98 to 44.68 €/MWh. These costs represent a reduction of up to 11.6% in the LCOS €/kgH_2, and one of up to 13.1% in the LCOS €/MWh for the high electricity cost scenarios. In the low-electricity-cost scenario, these respective reductions in LCOS are 9.1% and 10.6%.

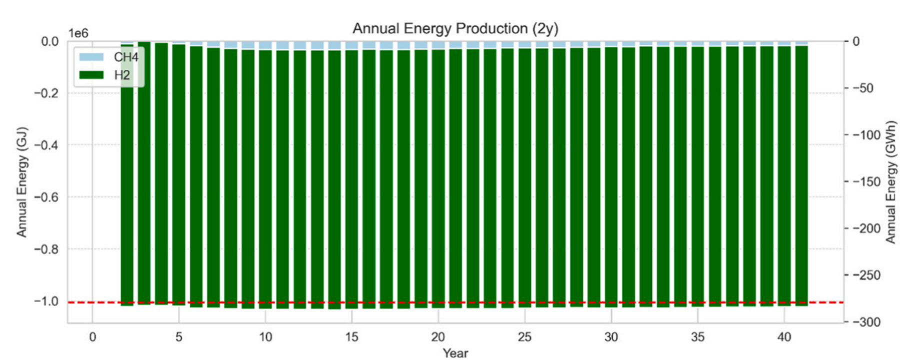

Fig. 4. Annual energy outputs from Scenario B in which the injection of cushion gas is spread over the first two annual cycles.

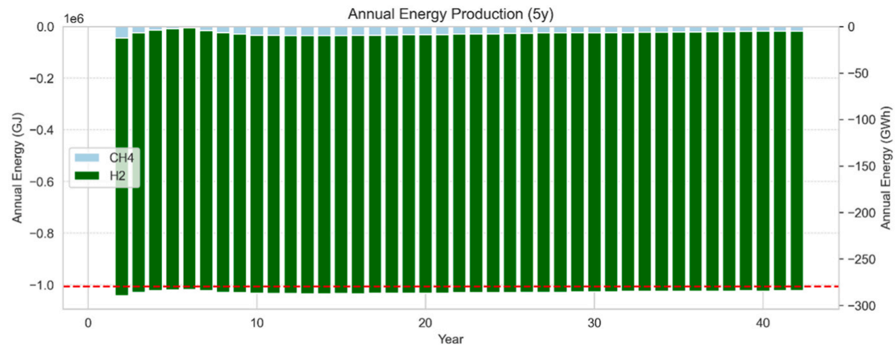

Fig. 5. Annual energy outputs from Scenario C in which the injection of cushion gas is spread over the first five annual cycles. The initial 3 years are now much more comparable to the long-term performance of the system. This might imply that this case is a good middle ground providing both cost savings and easier design due to a more consistent withdrawn mixture.

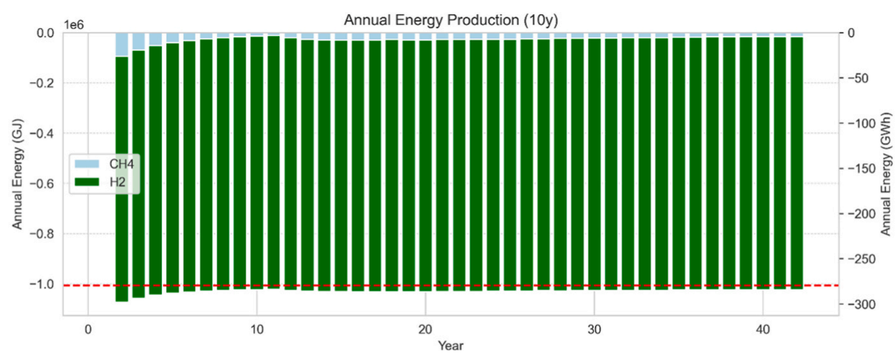

Fig. 6. Annual energy outputs from Scenario D in which the injection of cushion gas is spread over the first ten annual cycles. The initial years result in significantly more CH_4 energy being withdrawn from the reservoir compared to Scenario A. However, the long-term performance is not significantly altered.

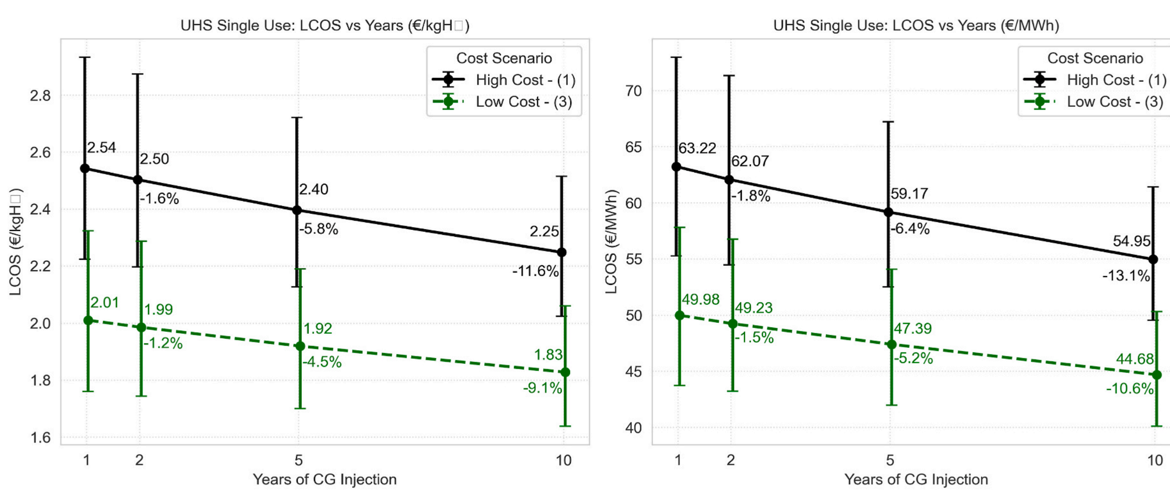

Fig. 7. LCOS results of UHS Single Use (no CO_2 storage) Scenario (1) with high electricity cost and Scenario (3) with low electricity cost, presented in terms of H_2 storage and in terms of energy storage.

3.2.2. Multi-use

For LCOS (€/kgH_2), the high-electricity-cost scenario (2) shows values decreasing from 2.90 €/kgH_2 when all the CG is injected in Year 1 to 2.61 €/kgH_2 when its injection is spread over ten years, an absolute reduction of 0.29 €/kgH_2. The low-electricity-cost scenario (4) ranges from 2.37 €/kgH_2 to 2.19 €/kgH_2 over the same period, corresponding to an absolute reduction of 0.18 €/kgH_2.

The corresponding energy LCOS (€/MWh) follows a similar trend, with the high-electricity-cost scenario decreasing from 72.20 to 63.86 €/MWh and the low-electricity-cost scenario from 58.97 to 53.58 €/MWh (a reduction of 8.34 and 5.39 €/MWh respectively). These costs represent a reduction of up to 10.0% in LCOS €/kgH_2 and up to 11.6% in LCOS €/MWh for the high electricity cost scenario. In the low-electricity-cost scenario, these respective reductions in LCOS are 7.6% and 9.1%.

For LCOS (€/kgCO_2), which is only reported for multi-use configurations, the high electricity cost scenario decreases from 0.187 €/kgCO_2 to 0.168 €/kgCO_2, an absolute reduction of 0.019 €/kgCO_2, while the

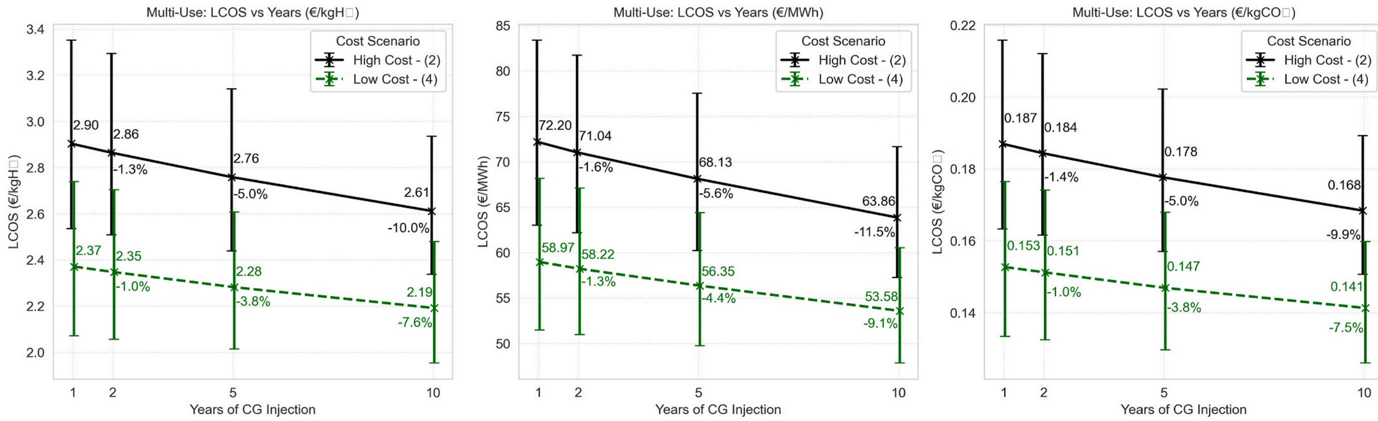

Fig. 8. LCOS over years of injection for the Multi-Use scenarios (2) and (4).

low electricity cost scenario decreases from 0.153 €/kgCO_2 to 0.141 €/kgCO_2, corresponding to an absolute reduction of 0.012 €/kgCO_2. These changes represent reductions of 9.9% and 7.5%, respectively.

4. Discussion

4.1. Staggering cushion gas lowers LCOS without degrading long-term performance

Stable long-term energy deliverability is achieved across all mechanistic scenarios (A–D). Once the storage reservoir is fully primed, the annual gas withdrawals of 350 million stdm^3 per year converge to a tight plateau of $\sim$1.03 PJ yr^{-1} with minimal drift. In the steady phases post CG injection, Scenario A sustains -1.027 ± 0.003 PJ yr^{-1} (trend = +0.063 TJ yr^{-1}); B holds -1.028 ± 0.004 PJ yr^{-1} (trend = +0.15 TJ yr^{-1}); C maintains -1.029 ± 0.004 PJ yr^{-1} (trend = +0.30 TJ yr^{-1}); and D delivers -1.028 ± 0.003 PJ yr^{-1} (trend = +0.28 TJ yr^{-1}). These results indicate that extending the injection of the cushion gas over five or ten years does not erode energy output over the 40 years simulated.

Early-cycle mixing and composition swings are observed in the H_2 reservoir. The H_2 injection into the residual CH_4 inside the reservoir introduces transient $H_2 - CH_4$ mixing that is most prominent when the injection of the cushion gas occurs over a long period (i.e., when the total injection of 1.4 or 1.2 kg s^{-1} is close to the working gas injection of 1 kg s^{-1}). In D (10-year CG injection), CH_4 supplies $3.67 \pm 2.52\%$ of the withdrawn energy during years 1–10, reaching up to 8.87%, before contracting to $2.33 \pm 0.48\%$ in balanced operation (years 11–41). In C (five-year ramp), early CH_4 is $1.90 \pm 1.54\%$ (0.50–4.32%) of the energy, settling to $2.64 \pm 0.59\%$ thereafter. Injection of cushion gas over a shorter period shows lower variations in the components' contribution to withdrawn energy: Scenario B averages $0.6 \pm 0.7\%$ from CH_4 during the first two cycles, then aligns with A at $\sim 2.46 \pm 0.69\%$ in the plateau. This behaviour is consistent with initial mobilisation of residual CH_4 followed by compositional stabilisation once the H_2 working inventory dominates. These results also indicate that allowing a H_2–CH_4 mixture during the CG injection phase might offer lower levels of CH_4 once the UHS operations are fully established and the hydrogen economy is well established.

Earlyyears see an increase in energy output due to the mobilisation of residual CH_4. Because CH_4 carries more energy per unit volume than H_2, periods with higher CH_4 fractions can lift early withdrawals modestly. In Scenario D, the CG injection decade averages -1.037 ± 0.017 PJ yr^{-1}, about 9 TJ yr^{-1} more energy than the later plateau (-1.028 PJ yr^{-1}). In C, convergence is quicker: -1.026 ± 0.010 PJ yr^{-1} during years 1–5 versus -1.029 ± 0.004 PJ yr^{-1} thereafter (a $\leq$3 TJ yr^{-1} difference). In A and B the system reaches the $\sim$1.03 PJ yr^{-1} plateau within $\sim$2 years, with initial deficits of $\sim$8 TJ yr^{-1} relative to the long-run mean. Overall, the extra early-year energy when the cushion gas is injected over 5 or 10 years is modest (sub-1% of annual energy output) and fades as mixing declines. Nevertheless, it is comparable to the $\sim$16 TJ required for the H_2 compression, and hence could help alleviate those costs in early years.

LCOS lowering is achieved through discounted cash-flow effects whilst capitalising on increased energy withdrawal due to residual natural gas. From a time-value-of-money perspective, lowering OCC will always reduce LCOS because early expenditures are discounted over a longer period (see the Methodology section). We expect that this phased approach also allows the geological reservoir to reach full operational maturity just as above-ground H_2 supply chains expand, forecast for the late 2030s and early 2040s [51]. The recovered energy composition evolution matches a pragmatic transition narrative. Specifically, in earlier years, when natural-gas value chains and offtake are mature, the energy stream contains a higher CH_4 share (up to $\sim$9% in D) but as H_2 markets, infrastructure and end-uses scale up, the energy content of the stream stabilises at $\sim$97–98% H_2 (steady-state CH_4 $\sim$2.3–2.6%), easing purity management and contracting.

Because the marginal cost of electrolyser-based H_2 is strongly influenced by electricity prices, the timing and volume of electrolyser-based H_2 cushion gas injections become key drivers of overall LCOS. In high electricity price regions, where H_2 is correspondingly expensive (Eq. (4)), cushion gas represents a large share of the capital expenditure, so any strategy that spreads out cushion gas injection over multiple years has a pronounced effect on LCOS. In contrast, in low electricity price systems, H_2 is cheaper and the relative importance of cushion gas in the LCOS is reduced, which helps to explain the different magnitudes of the cost impacts observed between the two electricity price regimes.

This relationship is captured in Eq. (4), where H_2 cost scales with electricity price and the energy required for electrolysis ($\approx$39.44 kWh/kgH_2). The function $g(\text{cost}_{\text{electricity}}, i)$ acts as a weighting factor between 0 and 1, describing the proportion of the H_2 production cost that electricity represents, reflecting that electricity price is not the sole determinant of H_2 production cost. At lower electricity prices, g tends to be closer to 0 because other factors—such as fixed costs, utilisation rates, and system efficiency—dominate. At higher electricity prices, g approaches 1, indicating that electricity becomes the primary driver of H_2 cost. This formulation ensures that the equation captures the combined influence of electricity price and operational constraints rather than attributing H_2 cost exclusively to electricity price.

Taken together, the production plateau (-1.028 to -1.029 PJ yr^{-1}; CV $\leq$ 0.40%) and the uniform LCOS decline across all scenarios (Figs. 7 and 8) show that deferring cushion-gas investment by up to a decade both preserves long-term performance and reduces LCOS by up to 11.6% (€/kg_{H2}) to 13.1% (€/MWh). The larger percentage reduction on an energy basis (€/MWh), compared to a mass basis (€/kg_{H2}), is consistent with the higher volumetric energy content of CH_4 relative to H_2. By this effect early-phase CH_4 mixing yields slightly more MWh per unit volume of gas recovered from the store, lowering the energy-normalised LCOS. The operational penalty consisting of transient composition swings diminishes naturally as the store matures and aligns with a developing H_2 value chain and reduction in greenhouse gases over the next couple of decades. The results of this part of the study highlight the validity of our first hypothesis, i.e., that the system can be engineered to avoid the degradation of the long-term performance of the UHS when injecting the cushion gas over multiple years. In addition, the initial fluctuations in gas composition remain manageable at a reasonable cost, with less than 0.03 and 0.04 percentage points of variation in LCOS (€/kg_{H2} and €/MWh respectively) when scaling the OPEX to account for these variations relative to an assumed constant OPEX value across scenarios. This demonstrates a novel approach to handling the deployment of cushion gas without impeding the long-term sustainability of the storage operation and underpins the economic discussion in the next section.

4.2. Co-locating CO_2 storage with UHS – what are the benefits?

The co-located CO_2 storage service LCOS of approximately 22 €/t_{CO2} is comparable to a mid-range cost from published values ranging from 1.8 to 35.3 €/t_{CO2} [52,53]. This value reflects the cost of the storage operation only and should not be conflated with the total cost of CO_2 capture, compression, and transport, which would raise the full CCS chain cost to somewhere in the range of 29.2 to 176.0 €/t_{CO2}, consistent with ranges reported for depleted field storage in the literature [52]. As there is no compressor in the CO_2 storage configuration, the storage LCOS shows little dependence on the electricity price scenario, remaining at 22 €/t_{CO2} between the high- and low-power cases. However, this near-constant absolute cost translates into different proportional increases in H_2 LCOS in the two regions, because the underlying H_2 cost base differs.

In the high-electricity-cost multi-use case (scenario series 2), we compared the four Monte Carlo LCOS distributions for scenarios A–D, corresponding to cushion-gas injection over 1, 2, 5, and 10 years, using a Kruskal–Wallis test. This non-parametric comparison was used because the LCOS outputs were not assumed to be normally distributed. Effect size was quantified using epsilon squared (ε^2), which indicated that the choice of cushion-gas injection schedule explained approximately 15% of the variation in ranked LCOS values. In practical terms, this effect is expressed mainly as a shift in the centre of the LCOS distribution: spreading cushion-gas injection from 1 year (A) to 10 years (D) lowers the median LCOS from 2.90 to 2.61 €/kg_{H2}, a reduction of 0.29 €/kg_{H2}. The uncertainty spread of each scenario is shown separately by the P10–P90 ranges in Fig. 8. This is notable because, although electricity prices are largely outside the operator's control [54], the cushion-gas injection schedule is an internal design lever that can materially reduce expected LCOS. This saving compensates some of the added cost of co-locating CO_2 storage, which raises LCOS by 0.36 €/kg_{H2}, so that the net cost of adding CO_2 storage when the cushion gas is injected over 10 years is only 0.07 €/kg_{H2}, corresponding to a relative increase of around 3% compared with the H_2-only case with all cushion gas injected in year one – the current most common and most investigated form of developing a UHS reservoir in porous reservoirs. That small premium could be offset by charging as little as 5 €/t_{CO2} for the CO_2 storage service, allowing the operator to either convert the remaining 17 €/t_{CO2} out of the 22 €/t_{CO2} storage LCOS into profit, or make CO_2 storage more cost-competitive and bring the whole CCS supply chain LCOS closer to a carbon price similar to the Emissions Trading Scheme (ETS) credit value of ~80€/ton in 2024. Crucially, this cross-subsidy works only one way: the cost of CO_2 storage itself cannot be reduced by spreading the cushion gas over multiple years as there is no cushion gas in that service. So, there is no analogous "saving" on the CO_2 side that could be passed back to H_2 storage.

In low electricity price markets, such as our scenario (4) case with mean electricity costs of 35 €/MWh, the economics of spreading the injection of cushion gas looks quite different. Because H_2 is cheaper in this scenario due to low electricity cost, the cost saving from spreading cushion gas injections over time is reduced. Specifically, we find a reduction of 0.18 €/kg_{H2} relative to the year-one cushion gas emplacement case (front-loaded case). In this low-electricity-cost case, the Kruskal–Wallis comparison across scenarios A–D (1, 2, 5, and 10 years of cushion-gas injection) gave an effect size of $\varepsilon^2 \approx 0.08$, indicating that the injection schedule explains only about 8% of the variation in ranked LCOS values. In practical terms, this corresponds to a modest shift in the centre of the LCOS distribution, with the median decreasing by 0.18 €/kgH_2 between the 1-year and 10-year cases, rather than a large change in distribution spread. At the same time, the added cost of providing co-located CO_2 storage remains at 0.36 €/kg_{H2}, so the saving from injecting cushion gas over a decade does not compensate for the CO_2 storage premium. The net cost of adding CO_2 storage when cushion gas is injected over 10 years is therefore 0.18 €/kg_{H2}, corresponding to a 9% increase relative to the H_2-only with all cushion gas in the 1st year baseline. Offsetting this much larger premium would require a CO_2 storage fee of approximately 12 €/t_{CO2}, which would leave only around 10 €/t_{CO2} out of the 22 €/t_{CO2} as profit. The ability of UHS to subsidise CO_2 storage without increasing the net cost of UHS operations thus diminishes by about 40% in low electricity-price settings.

Across both high and low electricity-price regimes, using CO_2 storage fees alone to pay for the UHS infrastructure is infeasible. Recovering the full UHS cost solely from CO_2 revenues would require storage tariffs in the range of ~140–185 €/t_{CO2}, far exceeding current and projected prices in the EU ETS and at the high end, or exceeding, typical estimates for the full CCS chain cost 30 – 176 €/t_{CO2} [52]. Such levels would be uncompetitive with alternative decarbonisation options and are unlikely to be politically or economically acceptable. This underscores that co-located CO_2 storage is the primary beneficiary of co-location rather than UHS. Although, in high electricity-price settings, CO_2 storage can also be viewed as a complementary revenue stream that can partly offset UHS costs.

Beyond the direct cost interactions quantified above, co-locating CO_2 storage with UHS also creates a distinct strategic advantage for H_2 production by steam methane reforming (SMR) with carbon dioxide capture in cases where bulk H_2 storage is of value. In the modelled system, the geometry of the storage complex allows for the annual storage of 118% of the CO_2 generated using SMR to produce the H_2 cushion gas. By providing a dedicated CO_2 storage sink, the dual-service facility enables "SMR H_2" used as cushion gas to be rendered effectively net-zero in less than a year of injection. This means that operators of co-located systems could access a cheap source of H_2 for cushion gas, potentially allowing a region with a diversity of H_2 producer technologies to benefit from a centralised storage system. However, our low electricity-price case study shows that when H_2 is cheaper, the incremental benefit of staggering cushion gas injections is greatly reduced, so there is an inherent feedback between the choice of H_2 production pathway and the value of staggering cushion gas. In addition, geological storage is expected to degrade H_2 purity [19], which may make sense to store lower-purity SMR H_2 rather than high-purity electrolyser-based H_2, particularly if SMR plants already possess gas purification infrastructure that could be shared with storage operations. Future work should therefore clarify the boundaries between SMR producers, storage operators, and H_2 off-takers, and systematically explore how these techno-economic feedbacks and potential cost savings are allocated among the different actors.

5. Conclusions

SSTs in general and large-scale storage in particular are critically important for developing and operating sustainable low-carbon energy systems. In this study we introduce a multi-use vision of a subsurface storage hub. We consider both the spatial and temporal dimensions of the multi-use case. Spatially, we assume that CO_2 storage and UHS operations can be co-located at the land surface, and in the deep subsurface the natural gas and H_2 storage can share the same geological storage reservoir. Temporally, we carefully consider the transition dynamics as energy system needs and decarbonisation targets are met.

Using mechanistic modelling of gas injection and withdrawal along with economic analyses, we demonstrated how phasing the emplacement of the H_2 cushion gas ($\geq$5 years) reduces LCOS by ~3.4–13.2% and smooths early cash requirements, aiding bankability without compromising energy output. We found that early composition swings in withdrawn gas are measurable (e.g., up to ~9% CH_4 energy share) but diminish with time, hence not impairing long-term forecasting and operations. Steady-state CH_4 energy in the withdrawn H_2 settles to near 2.3 to 2.6%, simplifying gas-quality management.

We illustrated how the co-location of UHS and CO_2 storage offers the possibility of deploying the cushion gas required for UHS operations over multiple years which can lead to a reduction of the CO_2 storage cost on a €/t_{CO2} basis.

Overall, a phased conversion of partially depleted gas reservoirs to H_2 storage service, co-located with CO_2 storage, offers a technically stable and economically advantageous route to seasonal storage that is aligned with near-term market realities and long-term decarbonisation objectives. It also offers flexibility in when to transition to a full UHS system in step with the growth of the hydrogen economy.

Declaration of generative AI and AI-assisted technologies in the manuscript preparation process

ChatGPT was used to improve and make the text more concise. The text provided to ChatGPT was paragraphs or snippets written by the authors and the outputs were reviewed and edited by the authors. The authors take full responsibility for the content of this article.

CRediT authorship contribution statement

Julien Mouli-Castillo: Conceptualization, Data curation, Formal analysis, Funding acquisition, Investigation, Methodology, Software, Validation, Visualization, Writing – original draft, Writing – review & editing. **Curtis M. Oldenburg:** Conceptualization, Methodology, Software, Supervision, Writing – original draft, Writing – review & editing. **Keni Zhang:** Software, Writing – review & editing. **Hanna Breunig:** Conceptualization, Data curation, Funding acquisition, Methodology, Supervision, Writing – original draft, Writing – review & editing.

Declaration of competing interest

The authors declare that they have no known competing financial interests or personal relationships that could have appeared to influence the work reported in this paper.

Acknowledgments

This work was supported as part of the UKRI Postdoc Fellowship Guarantee grant “Characterisation of synergies in subsurface energy storage technologies to support

energy systems decarbonisation” ref. EP/X028402/1. The authors (H.M.B., C.M.O.) gratefully acknowledge support from the U.S. Department of Energy with Lawrence Berkeley National Laboratory under Contract No. DE-AC02-05CH11231 with LBNL. The United States Government retains, and the publisher, by accepting the article for publication, acknowledges that the United States Government retains a nonexclusive, paid-up, irrevocable, worldwide license to publish or reproduce the published form of this manuscript, or allow others to do so, for United States Government purposes.

Appendix A. Supplementary data

Supplementary data to this article can be found online at https://doi.org/10.1016/j.ijhydene.2026.156158.

References

[1] Miocic Johannes M, Alcalde Juan, Heinemann Niklas, Marzan Ignacio, Hangx Suzanne. Toward energy-independence and net-zero: the inevitability of subsurface storage in Europe. ACS Energy Lett 2022;7(8):2486–9. https://doi.org/10.1021/acsenergylett.2c01303.

[2] Elliott David. A balancing act for renewables. Nat Energy 2016;1(1):15003. https://doi.org/10.1038/nenergy.2015.3.

[3] IAEA (International Atomic Energy Agency). Non-baseload operation in nuclear power plants: load following and frequency control modes of flexible operation. IAEA Nuclear Energy Series 2018:1–190. https://www.iaea.org/publications/11104/non-baseload-operation-in-nuclear-power-plants-load-following-and-frequency-control-modes-of-flexible-operation.

[4] U.S. Department of Energy. Achieving the promise of low-cost long duration energy storage. *U.S. Department of Energy* (August); 2024. https://www.energy.gov/oe/storage-innovations-2030.

[5] Miocic Johannes M, Heinemann Niklas, Alcalde Juan, Edlmann Katriona, Schultz Richard A. Enabling secure subsurface storage in future energy systems: an introduction. In: Miocic JM, Heinemann N, Edlmann K, Alcalde J, Schultz RA, editors. *Enabling secure subsurface storage in future energy systems* 0; 2023.

[6] Mouli-Castillo Julien, Wilkinson Mark, Mignard Dimitri, McDermott Christopher, Stuart Haszeldine R, Shipton Zoe K. Inter-seasonal compressed-air energy storage using saline aquifers. Nat Energy 2019;4(2):131–9.

[7] DESNZ. Guidance health and safety in grid Scale electrical energy storage systems (accessible webpage). 2024.

[8] EIA. Electricity explained energy storage for electricity generation. 2025. https://www.eia.gov/energyexplained/electricity/energy-storage-for-electricity-generation.php?.

[9] Matos Catarina R, Carneiro Júlio F, Silva Patrícia P. Overview of large-scale underground energy storage technologies for integration of renewable energies and criteria for reservoir identification. J Energy Storage 2019;21(March 2018):241–58. https://doi.org/10.1016/j.est.2018.11.023.

[10] Mouli-Castillo Julien, Wilkinson Mark, Mignard Dimitri, McDermott Christopher, Stuart Haszeldine R, Shipton Zoe K. Inter-seasonal compressed-air energy storage using saline aquifers. Nat Energy 2019;4(2):131–9. https://doi.org/10.1038/s41560-018-0311-0.

[11] Epelle Emmanuel I, Obande Winifred, Udourioh Godwin A, Christianah Afolabi Inioluwa, Desongu Kwaghtaver S, Orivri Uzezi, Gunes Burcu, Okolie Jude A. Perspectives and prospects of underground hydrogen storage and natural hydrogen. Sustain Energy Fuels 2022;6(14):3324–43. https://doi.org/10.1039/d2se00618a.

[12] Chen Yuanke, Wu Ronghui, Hsu Po-Chun. Perspective on distributed direct air capture: what, why, and how? Npj Materials Sustainability 2025;3(1):1–7. https://doi.org/10.1038/s44296-025-00056-w.

[13] Haszeldine R Stuart. Carbon capture and storage : how green can black be? Science 2009;325.

[14] Allen Myles, Axelsson Kaya, Caldecott Ben, Hale Thomas, Cameron Hepburn, Hickey Conor, Mitchell-Larson Eli, Malhi Yadvinder, Otto Friederike, Seddon Nathalie, Smith Steve. The Oxford principles for net zero aligned carbon offsetting. *University of Oxford* (September; 2020. p. 15. https://www.smithschool.ox.ac.uk/publications/reports/Oxford-Offsetting-Principles-2020.pdf.

[15] IEAGHG. A brief history of CCS and current status. 1, https://ieaghg.org/docs/General_Docs/Publications/Information_Sheets_for_CCS_2.pdf; 2012.

[16] Smith SM, Geden O, Nemet GF, Gidden MJ, Lamb WF, Powis C, Bellamy R, Callaghan MW, Cowie A, Cox E, Fuss S, Gasser T, Grassi G, Greene J, Lück S, Mohan A, Müller-Hansen F, Peters GP, Pratama Y, Repke T, Riahi K, Schenuit F, Steinhauser J, Strefler J, Valenzuela JM, Minx JC. The state of carbon dioxide removal - 1st edition. The State of carbon dioxide removal. 2023. https://doi.org/10.17605/OSF.IO/W3B4Z.

[17] Mouli-castillo Julien, Hanna Breunig, Oldenburg Curtis M. A call to industry : unearthing synergies in subsurface storage technologies. Greenhouse Gases Sci Technol 2025:1–9. https://doi.org/10.1111/ghg.70002.

[18] Williams Harri, Piessens Kris, Barros Renata, Konieczyńska Monika, Fajfer Joanna. GeoConnect3d - Overall conclusions and recommendations. 2021.

[19] Muhammed Nasiru Salahu, Haq Md Bashirul, Shehri Dhafer Abdullah Al, Al-Ahmed Amir, Rahman Mohammad Mizanur, Zaman Ehsan, Iglauer Stefan. Hydrogen storage in depleted gas reservoirs: a comprehensive review. Fuel 2023;337(December 2022):127032. https://doi.org/10.1016/j.fuel.2022.127032.

[20] Oldenburg Curtis M, Pan Lehua. Porous media compressed-air energy storage (PM-CAES): theory and simulation of the coupled wellbore–reservoir system. Transport Porous Media 2013;97(2):201–21. https://doi.org/10.1007/s11242-012-0118-6.

[21] Pruess Karsten, Curtis M Oldenburg, George Moridis. TOUGH2 User's guide Version 2. 2012 *(No. LBNL-43134). Berkeley, CA*.

[22] Doughty Christine, Oldenburg Curtis M. CO2 plume evolution in a depleted natural gas reservoir: modeling of conformance uncertainty reduction over time. Int J Greenh Gas Control 2020;97(April):103026. https://doi.org/10.1016/j.ijggc.2020.103026.

[23] Lei Hongwu, Jun Li, Li Xiaochun, Jiang Zhenjiao. Numerical modeling of Co-Injection of N2 and O2 with CO2 into aquifers at the tongliao CCS site. Int J Greenh Gas Control 2016;54:228–41. https://doi.org/10.1016/j.ijggc.2016.09.010.

[24] Walsh R, Nasir O, Calder N, Sterling S, Avis J. Combining TOUGH2 and FLAC3D to solve problems in underground gas storage. Transport Porous Media 2018;123(3):501–19.

[25] Pan L, Oldenburg CM, Freifeld BM, Jordan PD. Modeling the aliso canyon underground gas storage well blowout and kill operations using the coupled well-reservoir simulator T2Well. J Petrol Sci Eng 2018;161:158–74.
[26] Zhang Y, Oldenburg CM, Zhou Q, Pan L, Freifeld BM, Jeanne P, Tribaldos VR, Vasco DW. Advanced monitoring and simulation for underground gas storage risk management. J Petrol Sci Eng 2022;208:109763.
[27] Oldenburg Curtis M, Finsterle Stefan, Trautz Robert C. "Correction to: water upconing in underground hydrogen storage: sensitivity analysis to inform design of withdrawal. Transport Porous Media 2024;151(4):857–8. https://doi.org/10.1007/s11242-024-02066-z (2024), 151, 1, (55-84), 10.1007/S11242-023-02033-0)." Transport in Porous Media.
[28] Geuzaine Christophe, Remacle Jean-François. Gmsh: a three-dimensional finite element mesh generator with Built-in Pre-and post-processing facilities. 2009. 0.
[29] Soave G. Equilibrium constants from a modified redlich-kwong equation of state. Chem Eng Sci 1972;27(6):1197–203.
[30] Corey At. The interrelationship between oil and gas permeabilities. Prod Mon 1954;19(1):38–41.
[31] van Genuchten M Th. A closed-form equation for predicting the hydraulic conductivity of unsaturated soils. Soil Sci Soc Am J 1980;44(5):892. https://doi.org/10.2136/sssaj1980.03615995004400050002x.
[32] Boon Maartje, Hajibeygi Hadi. Experimental characterization of H2/Water multiphase flow in heterogeneous sandstone rock at the core scale relevant for underground hydrogen storage (UHS). Sci Rep 2022;12(1):1–12. https://doi.org/10.1038/s41598-022-18759-8.
[33] Yekta AE, Manceau JC, Gaboreau S, Pichavant M, Audigane P. Determination of hydrogen–water relative permeability and capillary pressure in sandstone: application to underground hydrogen injection in sedimentary formations. Transport Porous Media 2018;122(2):333–56. https://doi.org/10.1007/s11242-018-1004-7.
[34] IEA. Quarterly average wholesale prices for selected regions 2018-2026. 2025.
[35] NESO. Levelised cost of green hydrogen. 2025.
[36] Ogden J. Modeling infrastructure for a fossil hydrogen energy system with CO2 sequestration. In: Greenhouse gas control technologies - 6Th international conference, vol. 1; 2003. p. 1069–74. https://doi.org/10.1016/b978-008044276-1/50169-0.
[37] Lukawski Maciej Z, Silverman Rachel L, Tester Jefferson W. Uncertainty analysis of geothermal well drilling and completion costs. Geothermics 2016;64:382–91. https://doi.org/10.1016/j.geothermics.2016.06.017.
[38] Schellekens J, Coen Leo Panterra. Waarde van Aardwarmte En Regionale Mogelijkheden [Value of Geothermal Energy and Regional Opportunities]. 2020.
[39] Yousefi Seyed Hamidreza, Groenenberg Remco, Koornneef Joris, Juez-Larré Joaquim, Shahi Mina. Techno-economic analysis of developing an underground hydrogen storage facility in depleted gas field: a Dutch case study. Int J Hydrogen Energy 2023;48(74):28824–42. https://doi.org/10.1016/j.ijhydene.2023.04.090.
[40] Liu Shuyang, Li Hangyu, Zhang Kai, Lau Hon Chung. Techno-economic analysis of using carbon capture and storage (CCS) in decarbonizing China's coal-fired power plants. J Clean Prod 2022;351(September 2021):131384. https://doi.org/10.1016/j.jclepro.2022.131384.
[41] Geitner Christian, Waesker Markus, Doetsch Christian. Compressor cost optimization based on extended annual load duration curves. Chem-Ing-Tech 2020;92(10):1626–31. https://doi.org/10.1002/cite.202000034.
[42] André Jean, Auray Stéphane, Wolf Daniel De, Mohamed Mahmoud Memmah, Antoine Simonnet. Time development of new hydrogen transmission pipeline networks for France. Int J Hydrogen Energy 2014;39(20):10323–37. https://doi.org/10.1016/j.ijhydene.2014.04.190.
[43] Dehdari Leila, Burgers Iris, Xiao Penny, Li Kevin Gang, Singh Ranjeet, Webley Paul A. Purification of hydrogen from natural gas/hydrogen pipeline mixtures. Separ Purif Technol 2022;282(PB):120094. https://doi.org/10.1016/j.seppur.2021.120094.
[44] Liemberger Werner, Groß Markus, Miltner Martin, Harasek Michael. Experimental analysis of membrane and pressure swing adsorption (PSA) for the hydrogen separation from natural gas. J Clean Prod 2017;167:896–907. https://doi.org/10.1016/j.jclepro.2017.08.012.
[45] Mivechian Ali, Majid Pakizeh. Hydrogen recovery from Tehran refinery off-gas using pressure swing adsorption, gas absorption and membrane separation technologies: simulation and economic evaluation. Kor J Chem Eng 2013;30(4):937–48. https://doi.org/10.1007/s11814-012-0221-y.
[46] Peters Max S, Timmerhaus Klaus D. Plant design and economics for chemical engineers. fourth ed. McGraw-Hill; 1991.
[47] Mishra Shruti Khadka, Freeman Gerad M, Ganguli Sumitrra, Huerta Nicolas J. Which factors dominate the levelized costs of subsurface hydrogen storage in Pennsylvania, United States. Int J Hydrogen Energy 2024;91(October):814–21. https://doi.org/10.1016/j.ijhydene.2024.10.189.
[48] Scottish Centre for Carbon Storage. Opportunities for CO2 storage around Scotland, vols. 1–56; 2009.
[49] The Royal Society. Large-Scale electricity storage. 2023.
[50] Zakeri Behnam, Syri Sanna. Electrical energy storage systems: a comparative life cycle cost analysis. Renew Sustain Energy Rev 2015;42:569–96. https://doi.org/10.1016/j.rser.2014.10.011.
[51] Patonia Aliaksei, Lambert Martin, Lin Ning, Shuster Mark. ET47-Underground-Storage-for-Decarbonisation. 2025.
[52] Budinis Sara, Krevor Samuel, Mac Dowell Niall, Brandon Nigel, Hawkes Adam. An assessment of CCS costs , barriers and potential. Energy Strategy Rev 2018;22 (May):61–81. https://doi.org/10.1016/j.esr.2018.08.003.
[53] Smith Erin, Morris Jennifer, Kheshgi Haroon, Teletzke Gary, Howard Herzog, Paltsev Sergey. International journal of greenhouse gas control the cost of CO2 transport and storage in global integrated assessment modeling. Int J Greenh Gas Control 2021;109:103367. https://doi.org/10.1016/j.ijggc.2021.103367.
[54] Zun Moe Thiri, Mclellan Benjamin Craig. Cost projection of global green hydrogen production scenarios. 2023. p. 932–60.